J. Eur. Opt. Society-Rapid Publ. 2026, **22**, 4
© The Author(s), published by EDP Sciences, 2026
https://doi.org/10.1051/jeos/2025052
Available online at: https://jeos.edpsciences.org

Journal of the European Optical Society-Rapid Publications

Recent advances and trends on lasers and nonlinear materials and sources for near-Infrared
Guest editors: Azzedine Boudrioua and Patrice Camy

REVIEW ARTICLE OPEN ACCESS

Power scaling of tunable, narrowband, non-resonant PPLN optical parametric oscillators

Weidong Chen[1,2], Li Wang[1,3], Subhasis Das[1,4], Gerhard Spindler[5], Tugba Temel[1,6], André Schirrmacher[7], Ivan B. Divliansky[8], Marcin Piotrowski[9], Oussama Mhibik[8], Edlef Büttner[10], Chen Cui[1,11], Robert T. Murray[6], Ge Zhang[2], and Valentin Petrov[1,*]

[1] Max Born Institute for Nonlinear Optics and Ultrafast Spectroscopy, 2a Max Born Str., 12489 Berlin, Germany
[2] State Key Laboratory of Functional Crystals and Devices, Fujian Institute of Research on the Structure of Matter, Chinese Academy of Sciences, Fuzhou, 350002 Fujian, PR China
[3] Anhui Institute of Optics and Fine Mechanics, Chinese Academy of Sciences, Hefei, 230031 Anhui, PR China
[4] Laser Laboratory, Physics Department, Burdwan University, 713104 Burdwan, India
[5] Untere Gaisäckerstr. 10, 79761 Waldshut-Tiengen, Germany
[6] Blackett Laboratory, Department of Physics, Imperial College London, Prince Consort Road, London SW7 2BW, UK
[7] CANLAS GmbH, Schwarzschildstr. 12, 12489 Berlin, Germany
[8] CREOL, College of Optics and Photonics, University of Central Florida, Orlando, Florida 32816, USA
[9] French-German Research Institute of Saint-Louis, ISL, 5, rue du General Cassagnou, 68301 Saint-Louis, France
[10] APE Angewandte Physik & Elektronik GmbH, Plauener Str. 163-165, Haus N, 13053 Berlin, Germany
[11] Research Center for Crystal Materials, Xinjiang Technical Institute of Physics and Chemistry, Chinese Academy of Sciences, 830011 Urumqi, PR China

Received 30 September 2025 / Accepted 3 December 2025

Abstract. We review our recent achievements with narrowband, nanosecond, non-resonant optical parametric oscillators based on periodically-poled $LiNbO_3$, which are pumped at 1064 nm and emit close to degeneracy in the near-IR part of the spectrum between 1860 and 2486 nm. The average output power has been scaled up to the 10-W level with tuning across 40 nm (signal) and 66 nm (idler) using transversely chirped volume Bragg gratings (VBGs) acting on the signal wave. The maximum total average output power (signal + idler) achieved with a narrowband VBG has reached 11.35 W at 20 kHz, corresponding to a conversion efficiency of 63%. In this case, the signal and idler bandwidths amount to 0.7 and 0.9 nm at ~1922 and ~2384 nm, respectively. The experimentally observed spectral narrowing is reproduced by numerical simulations based on a split-step method within the plane-wave approximation taking account pump depletion and back-conversion. Spatial effects are also incorporated in the model, taking into account the transversal intensity distributions, in order to better reproduce the input-output power characteristics.

Keywords: Non-resonant optical parametric oscillator, Periodically-poled lithium niobate, Volume Bragg gratings, Near-infrared parametric light sources.

1 Introduction

Nanosecond optical parametric oscillators (OPOs) represent one of the most efficient approaches for extending the wavelength coverage of existing powerful coherent laser sources operating in the Q-switched mode from the near- to the mid-infrared (mid-IR) part of the spectrum. However, their power scaling capability often suffers from unwanted back-conversion and spectral broadening. The compromised spectral selectivity of the output is a serious drawback not only in direct applications but also when pumping a second-stage in a cascade configuration for further frequency down-conversion deeper into the mid-IR beyond 5 μm [1]. The second stage can be again an OPO pumped by the near-IR signal or idler output of the first stage or alternatively difference frequency generation (DFG) utilizing both of them [1]. This stage relies on narrow bandgap, low-phonon energy non-oxide nonlinear crystals such as $ZnGeP_2$, $AgGaSe_2$, CdSe or orientation patterned GaAs (OPGaAs) which feature extended mid-IR transparency but typically require pump wavelengths above 1.5 μm to avoid two-photon absorption. These crystals exhibit relatively narrow pump spectral acceptance bandwidth [1]. On the positive side, as a consequence of their narrow

* Corresponding author: petrov@mbi-berlin.de

band-gap, they possess substantially higher second-order susceptibility compared to the oxide type nonlinear crystals employed in the first stage.

The non-resonant OPO (NRO), in which none of the waves are resonant and the signal- and idler-waves leave the cavity after just one round trip in opposite directions, can alleviate the degradation of the beam quality and conversion efficiency caused by back conversion which occurs in conventional resonant OPOs. One of the NRO cavity mirrors is highly reflective (HR) at the signal and highly transmissive (HT) at the idler wavelength, while the other cavity mirror has the opposite properties (HT signal/HR idler). In contrast to the conventional OPOs where this is just an option to reduce the oscillation threshold, the pump wave in a NRO must be retro-reflected through the cavity to propagate in both directions in order to realize the feedback for the signal and idler waves.

The idea of such a resonatorless parametric oscillator was suggested theoretically as early as 1970 as a non-collinear scheme (to avoid the use of dichroic mirrors) using $LiNbO_3$ [2], and realized experimentally in the same year as a collinear NRO (to utilize the higher parametric gain) using an α-HIO_3 crystal [3]. The optical components in this early realization consisted of retro-reflecting prisms and polarizers as alternatives to dichroic mirrors which was possible thanks to the type-II phase-matching chosen. With the availability of high quality, damage resistant dichroic mirrors, and having in mind that their design as long-pass filters is easier due to the absence of parasitic reflectivity bands, the generic scheme of a modern linear cavity NRO will look like Figure 1.

It shall be emphasized that the early interest in resonatorless OPOs or NROs was motivated in those years by the fact that in the absence of both suitable laser sources and nonlinear crystals, the parametric gain was insufficient for travelling-wave type optical parametric generation (OPG) without any cavity. In this sense the NRO shall be distinguished from a related idea suggested even earlier, in 1966, the so-called backward-wave or mirrorless OPO (MOPO) [4], experimentally demonstrated more than 40 years later in 2007 [5]. In the MOPO, the feedback is realized by counterpropagating waves which requires very large birefringence: thus while the original work suggested the use of a Se single crystal which exhibits huge birefringence but unfortunately also high residual absorption [4], the realization became possible through engineered quasi-phase-matching (QPM) in a $KTiOPO_4$ (KTP) crystal [5]. In contrast, the NRO is based on mirrors although no longitudinal modes exist in the cold cavity. The two concepts were compared in an early review paper in terms of threshold which was estimated to be much higher for the MOPO [6].

Unfortunately, the first publications on the NRO concept [2, 3] remained largely unknown and the same idea was "rediscovered" 20 years later in [7] where a type-I β-BaB_2O_4 (BBO) crystal was employed in a collinear scheme. This experiment revealed that a NRO can provide similarly high slope and conversion efficiency as a singly-resonant oscillator (SRO). In the same paper [7], also an original scheme employing an intracavity quarter-wave plate was suggested for a single output degenerate NRO.

While initially the NRO was considered for nanosecond pumping by frequency doubled Nd lasers in the green due to the higher parametric gain [2, 3, 7], another 15 years later it was realized using type-II KTP pumped at 1064 nm in a ring cavity [8, 9]. These authors preferred to use the term cross-resonant oscillator (CRO) to emphasize the fact that in the presence of a pump wave (hot cavity), certain phase relationships have to be fulfilled after one cavity round-trip. However, this conclusion appears to be related to their choice to use the same ring cavity mirrors for circulating the pump. This does not correspond to the original NRO design [2, 3] and is technically more challenging to realize both in ring and linear cavities. Nevertheless, under reasonable assumptions (undepleted plane-wave limit and continuous-wave (CW) pumping) the authors of [9] compared theoretically their CRO to a SRO in terms of threshold, built-up time, saturation, etc., and concluded that the CRO is characterized by less back conversion and stronger pump depletion than the SRO, shorter build-up time and weaker saturation, supporting this with experimental results in the nanosecond regime. Thus, while degradation of beam quality and conversion efficiency caused by back conversion will be intrinsically suppressed in an NRO because the intracavity intensity of both the signal and idler waves is reduced to a minimum, as could be expected the pump threshold will be higher compared to a conventional SRO with 100% feedback for one of the waves and a retro-reflected pump wave [8]. Nevertheless, the NRO is a very promising concept for power scaling.

Another practical advantage of the CRO or NRO compared to the SRO is the dual wavelength output, in particular when it comes to DFG in the second stage of cascade down-conversion schemes for the mid-IR spectral range [1]. This has been experimentally demonstrated in [8] using KTP in the CRO and CdSe for DFG. It is obvious that the NRO scheme (see Fig. 1) is also ideal for seeding at one of the wavelengths, including narrowband and single-frequency seeding. In this aspect the NRO can be in fact considered also as a multi-pass parametric amplifier and this has been experimentally realized in [10, 11] as a component of a complex, single-frequency nanosecond system with impressive tunability from the visible to the mid-IR. This experiment in fact supports the interpretation of the NRO as a resonatorless parametric device.

Maintaining a narrowband spectrum at high average power is still, however, challenging for an NRO just as for an SRO since the parametric gain bandwidth increases with the pump power beyond the DFG limit determined by the difference of the signal and idler group velocities [1], which further broadens the output spectrum if no spectral constraining elements are employed. Broad spectral extent of the pump wave for the second stage of cascade parametric frequency down-converters not only clamps the conversion efficiency but will result in broadband output in the mid-IR. Volume Bragg Gratings (VBGs) in bulk glass acting on the signal or idler wave in the first stage OPO can be an elegant solution with relatively low insertion losses and high damage resistivity in a compact cavity configuration. In addition, Transversely Chirped VBGs (TC-VBGs) can be used not only for spectral narrowing of the OPO output

but also to ensure tunable operation in these conditions [12]. The transparency of such photo-thermo-refractive glass makes the choice of the signal wavelength preferable.

In our previous work we demonstrated that QPM materials, such as periodically-poled $LiNbO_3$ (PPLN) and KTP (PPKTP) are ideally suited for use in NROs because of the high parametric gain they can provide [13, 14]. However, exactly for such QPM structures the output of a NRO is normally broadband due to the same polarizations of all three waves (Type-0 interaction), in particular close to degeneracy. We also established that the use of VBGs at the signal wavelength is simpler to implement and provides higher spectral contrast [13, 15] when compared to laser seeding [16–18], at least when single-frequency operation is not targeted. This is related to the continuing action of the VBG at increased power levels during the build-up process and the absence of transversal spectral narrowing dependence.

In this work we review our ongoing efforts on power scalable and tunable operation of nanosecond, narrowband PPLN NROs. Using TC-VBGs as spectral narrowing elements, tuning ranges of 1860–1900 nm for the signal wave and 2420–2486 nm for the idler wave are obtained with spectral bandwidths less than 2 nm. The total average output power of the tunable, narrowband PPLN NRO using 1-mm thick PPLN is successfully scaled up to 9.84 W at a pulse repetition rate of 30 kHz. Increasing the PPLN thickness to 3 mm enabled some energy scaling at safer pump levels in [15], however, the oscillation threshold increased and the conversion efficiency dropped. The use of both thicker (3-mm vs. 1 mm in [13]) and longer (50-mm vs. 25 mm in [15]) PPLN that recently became commercially available can produce simultaneously the lowest NRO threshold and the highest output (total average power of 11.35 W) and conversion efficiency (63%) in the narrowband regime (sub-1-nm bandwidths achieved through a fixed wavelength VBG), at minimum risk for optical damage [19]. The results in terms of output spectra are supported by numerical simulations based on a split-step method within the plane-wave approximation that accounts for pump depletion and back-conversion. Although diffraction is not included, spatial effects are incorporated in the model, taking into account the transversal intensity distributions, in order to better reproduce the input-output power characteristics.

2 Experimental setup

The PPLN-NRO is pumped at 1064 nm by a multi-longitudinal mode (spectral linewidth ~0.66 nm) Nd:YVO_4 master oscillator power amplifier (MOPA) laser system (Canlas GmbH), delivering a maximum average power of 21 W with a beam quality factor of M^2~1.15. The pulse duration varies roughly between 5 and 17 ns depending on the repetition rate that could be varied from 5 to 50 kHz. A half-wave plate and a polarizer are used to adjust the pump power whilst keeping other characteristics (pulse duration and spatial quality) constant. A Faraday isolator (FI) is employed to prevent optical feedback to the pump laser,

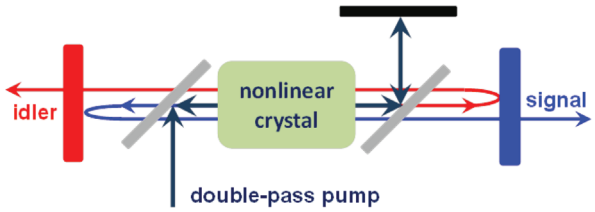

Figure 1. Generic scheme of a linear NRO.

and a second half-wave plate after the FI rotates the polarization to vertical for type-0 (eee) phase-matching in the PPLN crystal.

Two different anti-reflection (AR) coated 5% MgO doped PPLN slabs were employed, both supplied by HC Photonics Corp. (Taiwan). The first one had an aperture of 7.4 mm (wide) × 1 mm (thick) and a length of 20 mm, and contained triple gratings of 2 mm width but we used only the QPM period of 31.78 μm. Its residual reflectivity per surface was <0.1% for the pump and about 0.2% and 8% in the respective signal and idler ranges. The second, 3 × 3 mm^2 aperture, 50-mm long 5% MgO doped PPLN (Product OPMIR-SD) had a QPM period of 32.25 μm. Its measured surface reflectivity was 0.2% at the pump wavelength, 1.5% at the signal wavelength and 3.5% at the idler wavelength. Both samples had a parallelism specified as 3'. They could be heated in standard ovens (de facto a heater plate onto which the sample is fixed) supplied by the manufacturer with temperature control up to 200 °C.

The pump beam was focused into the thin PPLN crystal to a $1/e^2$ spot diameter of 590 μm by a spherical lens (f = 400 mm). For the thick PPLN the pump beam was down-collimated by an achromatic beam expander (GBE2-C, Thorlabs, USA) to a diameter of 1.26 mm (vertical) and 1.15 mm (horizontal) in the position of the crystal.

The signal output coupler was 95% reflective for the idler and 95% transmissive for the signal. The idler outcoupler was 99% reflective for the signal and 90% transmissive for the idler. The dichroic mirrors coupling the pump in and out of the NRO were highly transmissive for the signal (95%) and idler (91%) and highly reflective at the pump and its second harmonic. The pump retro-reflecting mirror was highly reflective at the pump and transmissive at 532 nm, enabling the double-pass pumping of the NRO and simultaneously outcoupling parasitic green second harmonic light due to higher order QPM.

Two commercial AR-coated TC-VBGs (OptiGrate, USA) with glass aperture 25 mm wide × 5.5 mm high but grating aperture 23 mm wide × 5 mm high were employed in the NRO with the thin PPLN substituting the idler output coupler, each of them with a tuning range of ±10 nm for the signal wave. Tuning is achieved by translating the TC-VBGs along their width. The TC-VBGs were 5.5 mm thick, with specified diffraction efficiency >96%. The reflectivity bandwidth was also certified by the supplier (~1 nm) but this parameter obviously depends on the beam size. The two TC-VBGs were selected in such a way in order to ensure a gapless tuning range of about 40 nm for the signal wave. The specified residual reflectivity for the signal wave was

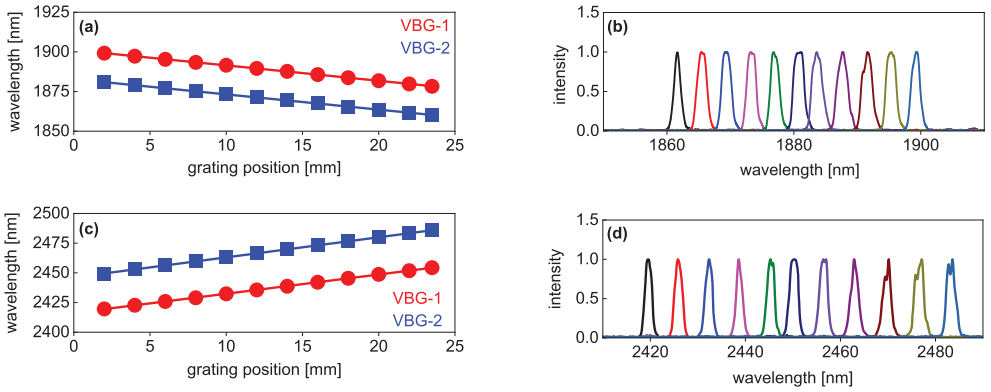

Figure 2. Spectral tuning of the narrowband NRO with the 1-mm thick PPLN and two TC-VBGs: (a) signal wave and (c) idler wave with linear fitting, and the corresponding spectra (b, d) recorded with a spectral resolution of 0.5 nm.

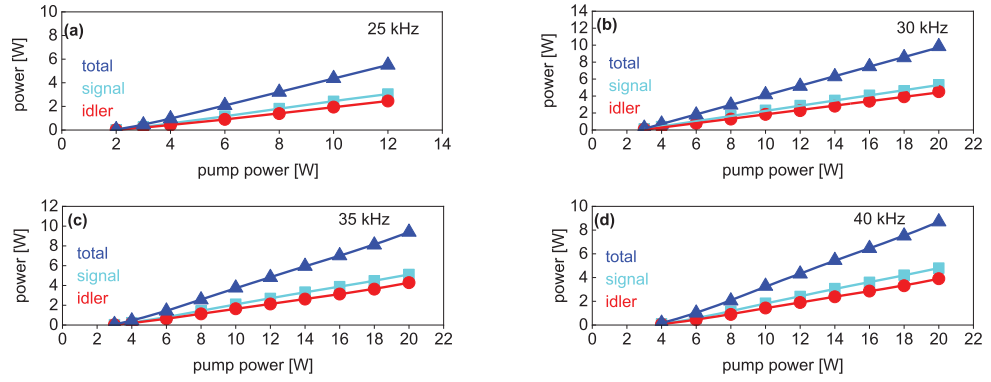

Figure 3. Input – output performance of the narrowband NRO with the 1-mm thick PPLN at different repetition rates: (a) 25 kHz, (b) 30 kHz, (c) 35 kHz, and (d) 40 kHz.

<0.5% and for the idler wave <0.75% per surface. For the thick PPLN, spectral narrowing was achieved by substituting the idler outcoupler by a home-made VBG centered near 1922 nm. This VBG had an aperture of 6×6.72 mm^2 and a thickness of 10.72 mm to ensure higher reflectivity. The estimated reflectivity bandwidth and diffraction efficiency were 0.5 nm and 99%, respectively. The fixed wavelength VBG was also double-side AR-coated for the signal and idler wavelengths and the measured residual reflectivity was 0.45% per surface for either of them.

The NRO cavity length (the physical distance between the two output couplers) was kept at minimum but this depended also on the crystal heater mount: The cavity length was ~50 mm for the 20-mm long PPLN and 135 mm for the 50-mm long PPLN. The dichroic 45° pump mirrors were mounted as close as possible to the PPLN crystal, and the retro-reflecting pump mirror – as close as possible to the second of them. All idler and signal powers were characterized using long-pass filters to eliminate residual light at shorter wavelengths.

3 1-mm thick PPLN: tuning and power scaling

The tuning performance and the power scaling potential of the PPLN NRO were first studied with the same 1-mm thick PPLN employed previously in [13]. Initially, a temperature of 169 °C was selected on the temperature controller corresponding to parametric down-conversion to ~1880 nm for the signal wave and 2453 nm for the idler wave. The average pump power was set at 3 W for a repetition rate of 20 kHz. At this pump level, the average output power of the signal wave amounted to 0.33 W and that of the idler wave to 0.29 W.

Spectral tuning was accomplished by transversal shifting the TC-VBGs across their width with a precision translation stage. The output power could be kept constant by adjusting the crystal temperature within roughly ±5°C. As can be seen in Figure 2, gapless tuning across 40 nm (1860–1900 nm) for the signal wave, Figure 2a, and across 66 nm (2420–2486 nm) for the idler wave, Figure 2c, was achieved. Linear fitting of the signal tuning data in Figure 2a gave a chirp rate of 0.96 nm/mm for the shorter wave TC-VBG and 0.97 nm/mm for the longer wave TC-VBG, in close agreement with the specifications. These values translate into 1.7 and 1.6 nm/mm in the corresponding idler wavelength tuning ranges. The simultaneously recorded signal spectra reveal a bandwidth (Full Width at Half Maximum, FWHM) of 1.4–1.9 nm, cf. Figure 2b, and for the idler the FWHM is in the 1.5–2.1 nm range, cf. Figure 2d. It can be seen that the spectral narrowing imposed to the signal wave by the TC-VBG is effectively

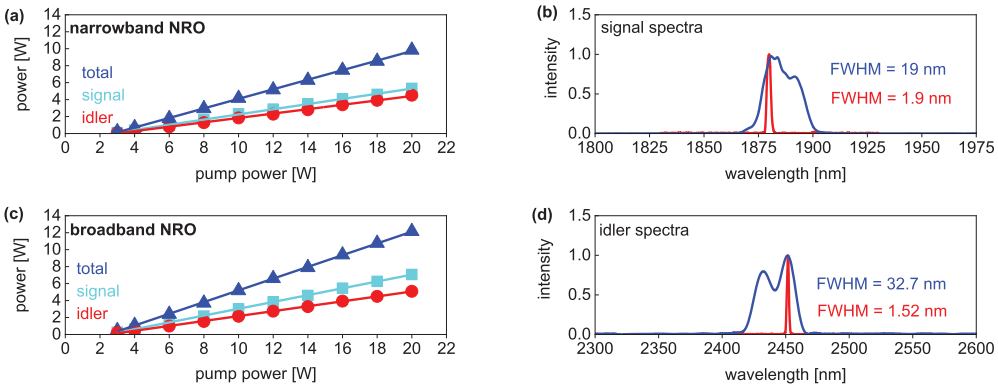

Figure 4. Comparison of narrowband and broadband NRO operation with the 1-mm thick PPLN in terms of measured input-output (a,c) and spectral (b,d) characteristics. The repetition rate is 30 kHz and the spectra in (b,d) were recorded at an average pump power of 7 W.

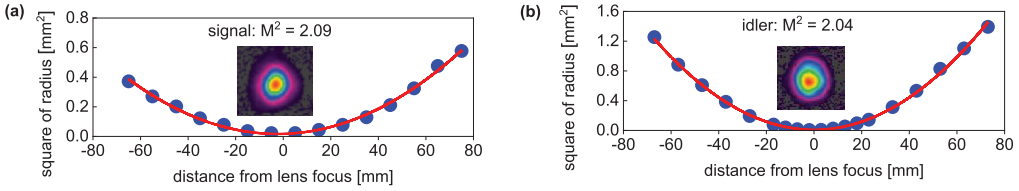

Figure 5. Spatial characteristics of the tunable, narrowband NRO with the 1-mm thick PPLN: measured (a) signal and (b) idler caustics in the horizontal plane with fitting for the evaluation of the M^2 propagation factor. The average pump power is 16 W at 30 kHz and the oven temperature is set to 169 °C corresponding to 1880 nm (signal) and 2453 nm (idler). The insets show recorded near-field beam profiles.

transferred to the idler wave, even though each of the waves is completely extracted in every cavity round trip in the NRO.

Power scaling of the narrowband NRO with the 1-mm thick PPLN was investigated at fixed signal (1880 nm) and idler (2453 nm) wavelengths, at an oven temperature of 169 °C. To utilize the full power available from the pump laser we had to increase the repetition rate, see Figure 3. Nevertheless, at 25 kHz we did not increase the pump level beyond 12 W, cf. Figure 3a, to avoid optical damage problems. In general, both the spatial and temporal characteristics of the pump laser change with the repetition rate. The shorter pulse duration at lower repetition rates, however, provides the best conditions for highest conversion efficiency and output powers due to the higher pump intensity. Thus, a maximum total average power of 9.84 W (5.32 W for the signal output and 4.52 W for the idler output) was obtained at the maximum pump level for a pulse repetition rate of 30 kHz, cf. Figure 3b. At an average pump power of 20 W, this corresponds to an optical conversion efficiency of 49.2% and a slope efficiency of 56.4%. The RMS stability of the average output power for the signal wave at 30 kHz, measured at a pump power of 16 W for 30 min, was 0.71%.

At the same pump conditions, substituting the TC–VBG by a signal reflecting mirror (idler outcoupler), as specified in the previous section, the output powers and efficiencies were higher in the broadband regime. Figure 4 shows a comparison at a repetition rate of 30 kHz. The

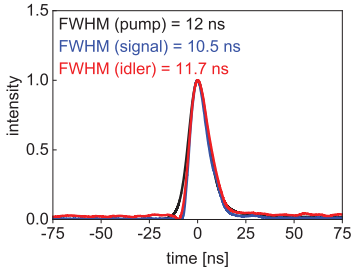

Figure 6. Temporal characteristics of the narrowband NRO with the 1-mm thick PPLN recorded with a 200-ps, extended InGaAs photodetector (FWHM indicated) at an oven temperature of 169 °C corresponding to emission wavelengths of 1880 nm (signal) and 2453 nm (idler). The average pump power is 16 W at 30 kHz.

maximum total average power in the broadband regime reached 12.16 W (7.07 W for the signal output and 5.09 W for the idler output). At an average pump power of 20 W, this corresponds to an optical conversion efficiency of 60.8% and a slope efficiency of 69.2%, see Figure 4c.

The signal and idler spectra for broadband and narrowband operation are compared in Figures 4b, 4d. Roughly 10-fold narrowing for the signal FWHM can be seen and about 20-fold for the idler FWHM.

The beam profiles for the signal and idler NRO outputs were measured by a Pyrocam PY-III-C-B camera

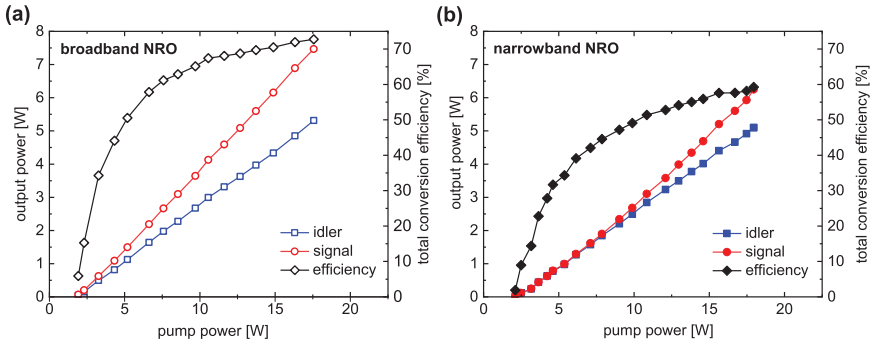

Figure 7. Signal and idler NRO average output powers for the 3-mm thick PPLN versus pump power at 20 kHz with the corresponding total conversion efficiency (signal + idler) for broadband (a) and narrowband (b) NRO operation.

(Ophir-Spiricon, USA) using a 300-mm CaF_2 focusing lens. The beam propagation factors (M^2) of the narrowband NRO with the 1-mm thick PPLN shown in Figure 5 were estimated from the fitted Gaussian diameters. We obtained $M^2 = 2.09$ for the signal beam and $M^2 = 2.04$ for the idler beam.

The pulse durations were measured at a pump level of 16 W, giving a FWHM value of 10.5 ns for the signal wave and 11.7 ns for the idler wave, slightly shorter than the pump pulse duration of 12 ns (Fig. 6).

4 3-mm thick PPLN: power/energy scaling at 20 kHz

In contrast to the previous section, using larger beam diameters in the 3-mm thick PPLN, it was possible to optimize the performance of the NRO at lower repetition rates which result in higher single pulse energies. Figure 7 shows the average signal and idler output powers at 20 kHz (corrected for the filters employed) versus pump power measured in front of the NRO (max: 17.95 W) at an oven temperature of 32 °C (chosen to match the VBG wavelength). This temperature was not changed further in the experiment.

The maximum signal (~1922 nm) and idler (~2384 nm) average powers at 20 kHz using the VBG reached 6.25 and 5.1 W, respectively, see Figure 7b. These average powers correspond to single pulse energies of 312.5 and 255 μJ, respectively. These results can be compared with [15] where we optimized the NRO at a repetition rate of 10 kHz for a similar 3-mm thick but only 25-mm long PPLN. The present threshold of 2.2 W is two times lower compared to [15] in terms of pump fluence for a similar number of cavity round trips. The maximum conversion efficiency (63%) is also almost two times higher compared to the 32.8% in [15]. The present single pulse energies at 20 kHz in fact exceed the maximum pulse energies achieved in [15] at 10 kHz. Comparing the NRO threshold for narrowband operation in Figures 7b and 4a, it can be seen that the values are similar in terms of single pump pulse energy but the threshold fluence is roughly four times lower for the 3-mm PPLN due to the larger beam sizes.

In the broadband regime (using the signal reflecting mirror instead of the VBG) at 20 kHz, the maximum conversion efficiency of the NRO with the 3-mm thick PPLN reached 72.8%, primarily due to increased signal output (7.5 W) with the idler almost unchanged (5.3 W) at a maximum pump level of 17.57 W, but the saturation behavior was more pronounced, see Figure 7a. The pump threshold for broadband operation was very similar (2.1 W).

All further NRO characteristics presented in this section were measured at maximum pump level. The measured spectral bandwidths (FWHM) recorded with the VBG in Figure 8b for the narrowband case, were limited by the spectrometer resolution. They were more than 20 times narrower compared to the broadband configuration with the signal reflecting mirror, cf. Figure 8a. In fact this estimation represents a lower limit because of the finite experimental spectral resolution in the narrowband case.

The fits for evaluation of the M^2 factors were performed with the second moment diameters. In the narrowband regime, at the maximum pump level at 20 kHz, we obtained $M^2 = 4.1$ for the signal and $M^2 = 2.7$–2.8 for the idler (see Fig. 9). The beam quality was inferior in broadband operation with measured $M^2 = 4.5$ (H) – 5.4 (V) for the signal and $M^2 = 3.6$ (V) – 4.1 (H) for the idler.

The signal pulse duration in narrowband operation roughly reproduced the pump pulse duration (7.5 ns) at 20 kHz, as shown in Figure 10. The pump temporal profile in Figure 10 shows some longitudinal mode-beating because the oscilloscope sampling bandwidth has not been reduced in these measurements, in contrast to Figure 6. The idler pulse was slightly longer (8.5 ns). In broadband operation with a signal reflecting mirror instead of the VBG, the output pulses were somewhat longer: 8.3 ns (signal) and 9.3 ns (idler).

5 Numerical modeling

The spectral distribution of the NRO output beams was simulated by a code widely following the split-step method #1 presented in [20] for plane waves. The mixing equations are integrated in the propagation direction in the time domain to account for the nonlinear parametric amplification ignoring dispersion, followed by a step taking into account the linear effects and in particular the temporal

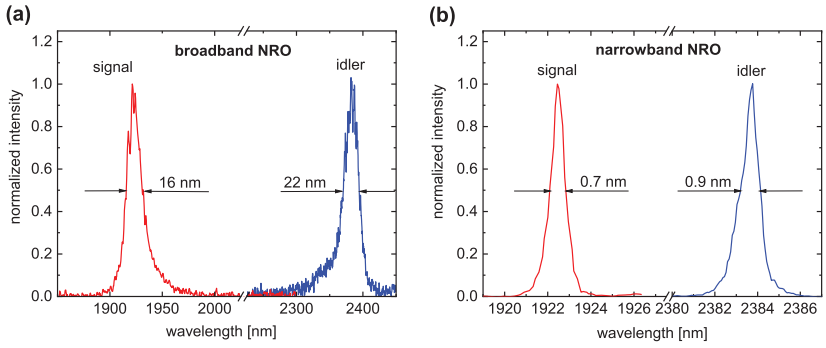

Figure 8. Signal and idler spectra of the NRO with the 3-mm thick PPLN at maximum pump level at 20 kHz recorded with a resolution of ~0.5 nm (FWHM indicated) for broadband (a) and narrowband (b) operation.

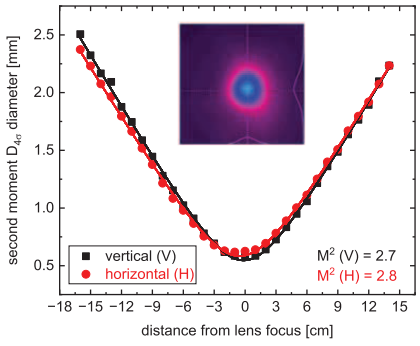

Figure 9. Idler beam caustics in the narrowband regime of the NRO with the 3-mm thick PPLN at maximum pump level at 20 kHz: experimental data (symbols) recorded with a Pyrocam PY-III-C-B camera (Ophir-Spiricon) using a 30-mm CaF_2 lens and fits (lines). The inset shows a far-field idler beam profile recorded at 1 m from the VBG.

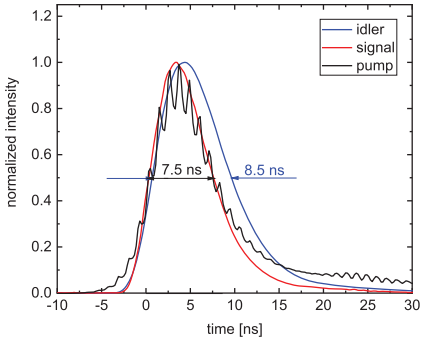

Figure 10. Pump, signal, and idler temporal profiles of the NRO with the 3-mm thick PPLN at maximum pump level at 20 kHz recorded with a 200-ps, extended InGaAs photodetector (FWHM indicated).

walk-off as a result of the group velocity mismatch (GVM) and the effect of group velocity dispersion (GVD) in the frequency domain. The actual spectral transmission and reflectivity of each mirror and the VBG are accounted for in a similar manner also in the frequency domain. The plane-wave model ignores diffraction but back conversion and pump depletion are its inherent features. No spatial walk-off effects are considered for QPM. The code starts with quantum noise generated in the standard way, i.e., by one half photon (signal, idler) energy per frequency interval on the average (electric field with random phase and Gaussian amplitude distribution with zero mean and corresponding variance).

For the 5 mol% MgO-doped $LiNbO_3$, the temperature-dependent Sellmeier relations from [21] are used. A direct evaluation of the effective nonlinearity of PPLN ($d_{\text{eff}} = 14$ pm/V) can be found in [22] and this value is widely quoted by manufacturers, including the present provider. It takes into account the imperfect poling quality of PPLN. According to [22] this value is considered to be 78% of the ideal value for a first order grating derived from $d_{33} = 28.2$ pm/V. The latter value for the diagonal tensor element agrees well with the $d_{33} = 25$ pm/V value reported for 5% MgO-doped congruent $LiNbO_3$ by non-phase-matched methods [23]. For our experimental conditions, we only converted the $d_{\text{eff}} = 14$ pm/V value valid for second-harmonic generation of 1064 nm fundamental to our three-wave parametric process using Miller's rule and the calculated refractive indices, which gave $d_{\text{eff}} = 11.8$ pm/V for use in the code.

When broadband radiation is considered, dispersion has to be accounted for in a similar way as for femtosecond pulse durations. The lowest order dispersion effect is equivalent to temporal walk-off between the signal and idler pulses in the time domain and this is an underlying mechanism in the code. The walk-off time between the signal and idler pulses is defined as usual in terms of the corresponding group velocities v_s and v_i given by $= \frac{c}{n_g}$, with the group refractive indices $n_g = n + \omega \frac{dn}{d\omega}$:

$$\tau_{s,i} = L_c \left| \frac{1}{v_s} - \frac{1}{v_i} \right|. \quad (1)$$

Here L_c denotes the crystal length. Temporal features with time scales shorter than $\tau_{s,i}$ are smoothed out by the GVM and cannot be correctly predicted by the model and this approximation is justified for spectral widths not exceeding $\tau_{s,i}^{-1}$ [23]. For yet larger spectral widths, the GVD terms in the coupled wave equations have to be retained.

Calculations for our experimental wavelengths with $L_c = 50$ mm yield $\tau_{s,i} = 0.67$ ps. This walk-off time is directly related to the spectral acceptance in the low parametric gain limit (DFG) assuming a narrowband pump wave, $\Delta\nu = 0.886/\tau_{s,i}$ which gives about 44 cm^{-1}, equivalent to 16 nm for the signal and 25 nm for the idler spectral bandwidths in the case of the 50-mm long PPLN. The parametric gain Γ broadens these values by a factor of ~$0.6 \times (\Gamma L_c)^{1/2}$ [1]. For the maximum pump level applied in the experiments with the 50-mm long PPLN crystal corresponding to a spatially averaged pump intensity of ~10.5 MW/cm^2, the increased parametric gain bandwidth is ~1.33×44 cm^{-1} = 59 cm^{-1} for a single pass parametric amplifier, i.e., only 33% larger compared to DFG. Although often used, these simple estimates ignore pump depletion and present an oversimplification being derived from analytical parametric gain expressions ignoring GVM and GVD, with the final results appearing ironically exactly in terms of GVM or, when the GVM is vanishing, in terms of the next term, GVD [1]. Strictly speaking all such analytical estimates are applicable for tunable monochromatic waves but not for ultrashort pulses or for broadband radiation in general. Usually, broadband nanosecond parametric oscillators will have narrower output bandwidths compared to the parametric amplification bandwidth due to multiple passes, however, saturation effects at higher conversion efficiency lead to the opposite trend. Thus, realistic estimations for the OPO and NRO output bandwidths, in particular taking into account depletion and back conversion, can be derived only from numerical simulations.

In the simulations we used the actual cavity mirror parameters from the experiments with the 50-mm long PPLN crystal. For normal incidence, we calculated the wavelength dependence of the diffraction efficiency (reflectivity) of the home-made VBG following the analytical formula presented in [24]. Alternatively, we modelled the VBG as a super-Gaussian ($n = 4$) shaped notch filter in the frequency domain. We established that the shape of this filter was not critical and the simulation results were mainly determined by its FWHM. Following [24], a FWHM of 0.5 nm and a peak reflectivity of 99% were assumed for the home-made VBG used.

The maximum pump power applied in the NRO experiments with the 50-mm long PPLN crystal corresponds to a pump pulse energy of 0.95 mJ. Thus, in the plane-wave simulations we used a spatially averaged peak pump intensity of ~10.5 MW/cm^2, equal to one half of the pump on-axis peak intensity. For the temporal shape of the pump pulse we assumed a Gaussian dependence with a FWHM of 7.5 ns in accordance with the experiment.

Alternatively, to emulate a Gaussian spatial pump beam distribution within the plane wave model while keeping the same temporal pump intensity dependence as in the true plane wave consideration we also used an approach we called quasi-spatial Gaussian (QSG). The beam computational area is divided into 10 annular segments of constant pump intensity corresponding to the Gaussian radial dependence. In the QSG simulation, the peak on-axis pump intensity is used as a parameter. For the experiment with the 50-mm long PPLN crystal, the maximum on-axis pump intensity amounts to 21 MW/cm^2, i.e., twice the average value used in the true plane wave approach. The $1/e^2$ pump beam radius is ~0.6 mm, as in the experiment, and the radial interval is chosen as 60.19 μm. The output energies are obtained by adding the contributions of all rings and the output spectra are obtained by a similar summation but using the ring areas (proportional to the radial distance from the beam center) as a weight function. The radial interval is chosen in such a way that for the chosen number of segments the pump intensity in the outermost ring is below the NRO threshold. We confirmed in preliminary tests that the final results converge at yet smaller intervals with larger number of segments.

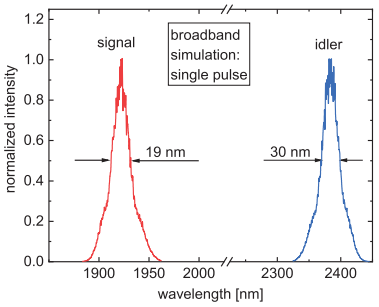

Figure 11. NRO output spectra for the 3-mm thick PPLN calculated for a single pulse using the QSG approach for broadband operation.

We established that the QSG approach leads to a closer agreement with the experimental results with respect to the input output energetic performance. Concerning the simulation of the NRO output spectra, essential deviations from the true plane wave approach were observed only in the broadband case with the spectra computed by the QSG approach being broader. No significant differences were observed in the narrowband case, which can be explained by the VBG acting as a very narrow frequency filter dominating all other spectral shaping effects. While in the true plane wave approach we averaged the final spectral results over multiple pulse simulations, in the QSG approach some spectral averaging takes place even when only one pump pulse is simulated.

Figure 11 presents the spectra obtained by such a single QSG simulation in the broadband case, and Figure 12a presents the spectra obtained by QSG simulation averaged over 10 pulses in the narrowband case for the 50-mm long PPLN crystal. The simulation provides output spectral data with high resolution corresponding to a wavelength step of ~0.01 nm for the signal and ~0.015 nm for the idler. The narrowband spectra were additionally smoothed to account for the finite experimental spectral resolution (~0.5 nm). This was realized by convolving the computed spectra with a Gaussian apparatus function with the corresponding FWHM in the frequency domain, followed by conversion to wavelength units to plot Figure 12b. In fact this smoothing procedure made the averaging over multiple pulses starting from quantum noise (i.e., multiple pulse simulations) redundant.

The simulation results provided strong support for the experimental observations in terms of spectral behavior demonstrating that the VBG acting on the signal wave

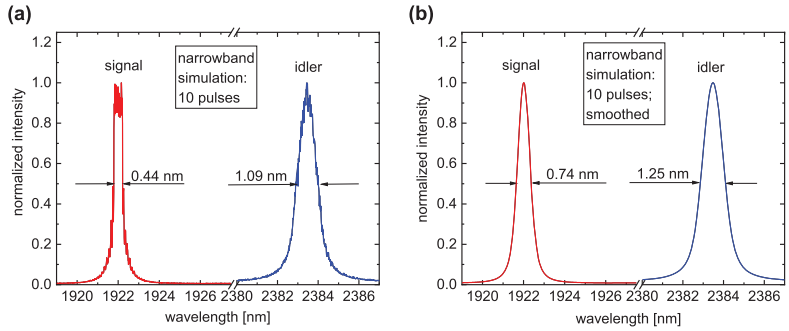

Figure 12. NRO spectra for the 3-mm thick PPLN calculated using the QSG approach for narrowband operation by averaging over 10 pulses (a) and with additional smoothing to simulate the experimental spectral resolution of 0.5 nm (b).

dramatically narrows both the signal *and* idler spectra, cf. Figure 12b. The spectral FWHMs estimated from the computational raw data in the narrowband case were 0.44 and 1.09 nm for the signal and idler, respectively. Then the actual spectral narrowing factor for the signal exceeds 40 while for the idler it is close to 30. The calculated bandwidth values increased to 0.74 and 1.25 nm, respectively, as a result of the smoothing with the spectrometer instrumental function, in good agreement with the recorded spectra shown in Figure 8b for the NRO signal and idler outputs. Somewhat larger deviation from the experimental spectra is observed for the idler spectral bandwidth, both in the broadband and in the narrowband cases, which is larger in the simulations. Finally, within the framework of the plane-wave model approach, it is not possible to make reliable statements on the absolute values of the output powers. Further, predictions of the beam profiles (beam qualities) are completely out of the scope of this numerical method and the present work.

6 Conclusion

Our recent studies with different samples of PPLN revealed that this material is ideally suited for application in 1-μm pumped non-resonant parametric oscillators to ensure maximum energy extraction in the nanosecond regime for both signal and idler. VBGs present a simple, robust and effective solution to narrow the bandwidths of both outputs although they act only on the signal wave. This is important not only for the spectral selectivity in direct applications but also for achieving high efficiency and narrow bandwidths in the mid-IR part of the spectrum by adding a second, cascade frequency conversion stage based on a non-oxide nonlinear crystal.

Using a 1-mm thin and 20-mm long PPLN sample and TC-VBGs for spectral narrowing, we achieved power scalable and simultaneously wavelength tunable operation of the NRO with a maximum total (signal plus idler) average power of 9.84 W at 30 kHz. Spectral tuning ranges of 40 nm for the signal and 66 nm for the idler wave were covered combining two such TC-VBGs. The spectral narrowing effect in this case depends on the beam size on the 20 mm wide TC-VBGs and the measured spectral bandwidths did not exceed 2 nm in the entire tuning range both for the signal and the idler outputs.

A conversion efficiency of 63% with a total (signal plus idler) output power of 11.35 W were achieved from the NRO in the narrowband regime using a 50-mm long PPLN crystal pumped at 20 kHz and a home-made, narrowband, fixed wavelength VBG. The larger aperture (3×3 mm^2) of this crystal enabled more flexible operation in terms of repetition rates to utilize the full available power from the specific pump source and the average powers obtained correspond to single pulse energies of 312.5 and 255 μJ for the signal and idler, respectively. At maximum pump/output levels, the bandwidths of both outputs were narrowed in this case to less than 1 nm although the signal and idler wavelengths (~1922 and ~2384 nm) were not far from degeneracy.

The NRO was modelled using a split-step method approach in the plane wave approximation applicable for broadband radiation, with excellent agreement between the numerical and experimental results in terms of spectral narrowing achieved by using VBGs. The actual spectral narrowing calculated for the signal wave exceeds a factor of 40. Spatial intensity distributions were considered in a simplified QSG extension of the same code which provided better agreement with the experimental data in terms of output energies and efficiency.

The maximum on-axis pump fluence applied in the experiments with the large aperture (3×3 mm^2) 50-mm long PPLN crystal was below 0.32 J/cm^2. For this estimation we took into account a factor of 2 for the double pass pumping which is inherent to the NRO concept. The above value is three times lower compared to the experiments with the 1-mm thick PPLN, in which comparable average output powers were achieved for lower (49.2%) conversion efficiency at a higher (30 kHz) repetition rate chosen for safe operation. The maximum on-axis fluence of 0.32 J/cm^2 translates into less than 100 MW/cm^2 for the peak on-axis intensity which is expected to ensure safe long-term operation for further extension of the present experiments towards a cascade frequency conversion configuration covering the mid-IR part of the spectrum beyond 5 μm. The achieved spectrally narrow outputs and the high average powers are prerequisites for efficient frequency conversion from the 2-μm range to the mid-IR spectral range.

The nonlinear crystal, most suitable for the high average power regime at multi-10-kHz repetition rates in the second stage, is OP-GaAs which, as a QPM material, has similar limitations in terms of available aperture as PPLN [1]. Apart from its numerous advantages in terms of extended transparency, nonlinearity and thermo-mechanical properties, OP-GaAs exhibits rather narrow pump acceptance bandwidth and will greatly benefit from the spectral narrowing achieved in the PPLN NRO [25, 26].

Further power scaling of the present NRO based on the large aperture 50-mm long PPLN crystal is obviously possible with more powerful (e.g., ~50 W) pump sources. Keeping the same pump levels in terms of fluence and intensity, e.g., at 20 kHz, from the comparison of the beam diameters in the two crystals employed in the present work, it is clear that the pump beam size in the large aperture PPLN can be simply increased by a factor of 1.5 which means that total energies exceeding 1 mJ and total average powers exceeding 20 W can be expected at similarly high conversion efficiency and minimum damage risk.

Funding

This project has received funding from DAAD (Germany) – DST (India) 2023-2025 project-related personal exchange programme (Grant no. 57683248) and the European Union's Horizon 2020 research and innovation programme under grant agreement no. 871124 Laserlab-Europe.

Conflicts of interest

The authors declare that they have no competing interests to report.

Data availability statement

Data underlying the results presented in this paper are not publicly available at this time but may be obtained from the authors upon reasonable request.

Author contribution statement

Conceptualization, W.C., L.W, V.P. and R.M.; Methodology, W.C., L.W.; Software, G.S. and M.P.; Validation, T.T., S.D. and C.C.; Formal Analysis, W.C. and V.P.; Investigation, W.C., L.W., S.D. and T.T.; Resources, A.S., I.D., O.M., E.B., G.Z. and R.M.; Data Curation, C.C. and T.T.; Writing – Original Draft Preparation, V.P.; Writing – Review & Editing, V.P., W.C., M.P. and G.S.; Visualization, T.T., W.C., L.W. and C.C.; Supervision, V.P., W.C., R.M. and G.Z.; Project Administration, V.P.; Funding Acquisition, V.P., S.D., and R.M.

References

1 Petrov V, Frequency down-conversion of solid-state laser sources to the mid-infrared spectral range using non-oxide nonlinear crystals, *Prog. Quantum Electron.* **42**, 1 (2015). https://doi.org/10.1016/j.pquantelec.2015.04.001.

2 Sushchik MM, Fortus VM, Freidman GI, A resonatorless parametric light oscillator, *Radiophys. Quantum Electron.* **14**, 211 (1971). https://doi.org/10.1007/BF01031402 [transl. from Izvestiya Vysshikh Uchebnykh Zavedenii, Radiofizika **14**, 263 (1971). https://radiophysics.unn.ru/sites/default/files/papers/1971_2.pdf].

3 Kovrigin AI, Nikles PV, Resonatorless parametric light generator using an α-HIO_3 crystal, *JETP Lett.* **13**, 313 (1971). http://jetpletters.ru/ps/0/article_24305.shtml [transl. from ZhETF Pis. Red. **13**, 440 (1971). http://jetpletters.ru/ps/0/article_11106.shtml].

4 Harris SE, Proposed backward wave oscillation in the infrared, *Appl. Phys. Lett.* **9**, 114 (1966). https://doi.org/10.1063/1.1754668.

5 Canalias C, Pasiskevicius V, Mirrorless optical parametric oscillator, *Nat. Photon.* **1**, 459 (2007). https://doi.org/10.1038/nphoton.2007.137.

6 Fischer R, Kulevskii LA, Optical parametric oscillators (review), *Sov. J. Quantum Electron.* **7**, 135 (1977). https://doi.org/10.1070/QE1977v007n02ABEH008850 [transl. from Kvantovaya Elektronika **4**, 245 (1977) https://www.mathnet.ru/eng/qe8850]; Erratum: Sov. J. Quantum Electron. **7**, 798 (1977). https://doi.org/10.1070/QE1977v007n06ABEH012910 [transl. from Kvantovaya Elektronika **4**, 2067 (1977). https://www.mathnet.ru/eng/qe15745].

7 Guyer DR, Lowenthal DD, Novel cavity design for a high-efficiency, high-energy near-infrared β-BaB_2O_4 parametric generator, *Proc. SPIE* **1220**, 41 (1990). https://doi.org/10.1117/12.18304.

8 Godard A, Raybaut M, Lambert O, Faleni J-P, Lefebvre M, Rosencher E, Cross-resonant optical parametric oscillators: study of and application to difference-frequency generation, *J. Opt. Soc. Am. B* **22**, 1966 (2005). https://doi.org/10.1364/JOSAB.22.001966.

9 Berrou A, Melkonian J-M, Raybaut M, Godard A, Rosencher E, Lefebvre M, Specific architectures for optical parametric oscillators, *C.R. Physique* **8**, 1162 (2017). https://doi.org/10.1016/j.crhy.2007.09.012.

10 Bosenberg WR, Guyer DR, Broadly tunable, single-frequency optical parametric frequency-conversion system, J, *Opt. Soc. Am. B* **10**, 1716 (1993). https://doi.org/10.1364/JOSAB.10.001716.

11 Lowenthal DD, 2-Micron optical parametric sources, *Proc. SPIE* **1864**, 190 (1993). https://doi.org/10.1117/12.146881.

12 Jacobsson B, Canalias C, Pasiskevicius V, Laurell F, Narrowband and tunable ring optical parametric oscillator with a volume Bragg grating, *Opt. Lett.* **32**, 3278 (2007). https://doi.org/10.1364/OL.32.003278.

13 Wang L, Boyko AA, Schirrmacher A, Büttner E, Chen W, Ye N, Petrov V, Narrow-band periodically poled lithium niobate nonresonant optical parametric oscillator, *Opt. Lett.* **44**, 5659 (2019). https://doi.org/10.1364/OL.44.005659.

14 Boyko AA, Wang L, Mhibik O, Divliansky IB, Zukauskas A, Moelster K, Chen W, Glebov LB, Pasiskevicius V, Petrov V, High-energy, narrowband, non-resonant PPKTP optical parametric oscillator, *Proc. SPIE* **11985**, 119850G (2022). https://doi.org/10.1117/12.2613384.

15 Temel T, Murray RT, Wang L, Chen W, Schirrmacher A, Divliansky IB, Mhibik O, Glebov LB, Petrov V, Energy scaling of a narrowband, periodically-poled $LiNbO_3$, nanosecond, non-resonant optical parametric oscillator. *Appl. Opt.* **63**, 1811 (2024). https://doi.org/10.1364/AO.514729.

16 Murray RT, Wang L, Chen W, Battle RA, Schirrmacher A, Büttner E, Petrov V, Narrowband seeding of a PPLN nonresonant optical parametric oscillator, *Proc. SPIE* **12405**, 1240508 (2023). https://doi.org/10.1117/12.2661705.

17 Temel T, Murray RT, Wang L, Chen W, Schirrmacher A, Battle RA, Petrov V, Narrowband-seeded PPLN non-resonant optical parametric oscillator, *Opt. Mater. Express* **14**, 889 (2024). https://doi.org/10.1364/OME.517919.

18 Temel T, Das S, Spindler G, Schirrmacher A, Murray RT, Piotrowski M, Wang L, Chen W, Petrov V, Power scaling of a narrowband-seeded, non-resonant optical parametric oscillator based on periodically-poled $LiNbO_3$, *Photonics* **12**, 743 (2025). https://doi.org/10.3390/photonics12080743.

19 Das S, Temel T, Spindler G, Schirrmacher A, Divliansky IB, Murray RT, Piotrowski M, Wang L, Chen W, Mhibik O, Petrov V, Power scaling of a non-resonant optical parametric oscillator based on periodically-poled $LiNbO_3$ with spectral narrowing, *Opt. Express* **33**, 5662 (2025). https://doi.org/10.1364/OE.550781.

20 Smith AV, Gehr RJ, Bowers MS, Numerical models of broad-bandwidth nanosecond optical parametric oscillators, *J. Opt. Soc. Am. B* **16**, 609 (1999). https://doi.org/10.1364/JOSAB.16.000609.

21 Gayer O, Sacks Z, Galun E, Arie A, Temperature and wavelength dependent refractive index equations for MgO-doped congruent and stoichiometric $LiNbO_3$, *Appl. Phys. B* **91**, 343 (2008). https://doi.org/10.1007/s00340-008-2998-2; Erratum **94**, 367 (2009). https://doi.org/10.1007/s00340-008-3316-8; Erratum **101**, 481 (2010). https://doi.org/10.1007/s00340-010-4203-7.

22 Miller GD, Batchko RG, Tulloch WM, Weise DR, Fejer MM, Byer RL, 42%-efficient single-pass cw second-harmonic generation in periodically poled lithium niobate, *Opt. Lett.* **22**, 1834 (1997). https://doi.org/10.1364/OL.22.001834.

23 Shoji I, Kondo T, Kitamoto A, Shirane M, Ito R, Absolute scale of second-order nonlinear-optical coefficients, *J. Opt. Soc. Am. B* **14**, 2268 (1997). https://doi.org/10.1364/JOSAB.14.002268.

24 Ciapurin IV, Drachenberg DR, Smirnov VI, Venus GB, Glebov LB, Modeling of phase volume diffractive gratings, part 2: reflecting sinusoidal uniform gratings, Bragg mirrors, *Opt. Eng.* **51**, 058001 (2012). https://doi.org/10.1117/1.OE.51.5.058001.

25 Vodopyanov KL, Makasyuk I, Schunemann PG, Grating tunable 4–14 μm GaAs optical parametric oscillator pumped at 3 μm, *Opt. Express* **22**, 4131 (2014). https://doi.org/10.1364/OE.22.004131.

26 Wang L, Chen W, Schunemann P, Schirrmacher A, Büttner E, Boyko AA, Ye N, Zhang G, Zhao Y, Petrov V, Nanosecond optical parametric oscillator with midinfrared intracavity difference-frequency generation in orientation-patterned GaAs, *Opt. Lett.* **46**, 332 (2021). https://doi.org/10.1364/OL.413583.